Elevated paleomagnetic dispersion at Saint Helena suggests long-lived anomalous behavior in the South Atlantic

Yael A. Engbers, Andrew J. Biggin, Richard K. Bono

Geomagnetism Laboratory, Dept. Earth, Ocean and Ecological Sciences, University of Liverpool

** Yael A. Engbers; Email: y.a.engbers@liverpool.ac.uk*

Physical sciences, Earth, Atmospheric and Planetary Sciences

South Atlantic Anomaly; reversals; secular variation; core dynamics; core-mantle boundary

Author Contributions AJB designed the research project. YAE and AJB collected the samples from Saint Helena. YAE carried out most experiments and analyses. All authors wrote the paper.

This PDF file includes:

Main Text
Figures 1 to 4

Abstract

The Earth's magnetic field is presently characterized by a large and growing anomaly in the South Atlantic Ocean. The question of whether this region of Earth's surface is preferentially subject to enhanced geomagnetic variability on geological timescales has major implications for core dynamics, core-mantle interaction, and the possibility of an imminent magnetic polarity reversal. Here we present paleomagnetic data from Saint Helena, a volcanic island ideally suited for testing the hypothesis that geomagnetic field behavior is anomalous in the South Atlantic on timescales of millions of years. Our results, supported by positive baked contact and reversal tests, produce a mean direction approximating that expected from a geocentric axial dipole for the interval 8-11 million years ago but with very large associated directional dispersion. These findings indicate that, on geological timescales, geomagnetic secular variation is persistently enhanced in the vicinity of Saint Helena. This in turn supports the South Atlantic as a locus of unusual geomagnetic behavior arising from core-mantle interaction while also appearing to reduce the likelihood that the present-day regional anomaly is a precursor to a global polarity reversal.

Significance

Earth's magnetic field is generated in the outer core by convecting liquid iron and protects the atmosphere from solar wind erosion. The most substantial anomaly in the magnetic field is in the South Atlantic. An important conjecture is that this region could be a site of recurring anomalies because of unusual core-mantle conditions but this has not previously been tested on geological timescales. With paleodirectional data from rocks from Saint Helena, an island in the South Atlantic, we show that the directional behavior of the magnetic field in the South Atlantic did indeed vary anomalously between ~8-11 million years ago. This supports the hypothesis of core-mantle interaction being manifest in the long-term geomagnetic field behavior of this region.

Main Text

Paleomagnetic records and geomagnetic observations show us that, except for brief intervals associated with reversals and excursions, the Earth's magnetic field is dominated by an axial dipole (1). Indeed, a long-standing hypothesis states that, if averaged over sufficient time (~10^4 – 10^5 years), the Earth's magnetic field approximates a dipole field that is aligned with the rotation axis of the Earth, called a geocentric axial dipole (GAD) (2). On shorter timescales and in the present day, there are spatially and temporally complex features (3–5) that must be averaged out over time for the GAD hypothesis to be valid. A primary example of these features is the South Atlantic Anomaly (SAA) (Figure 1), caused by a substantial patch of reversed magnetic flux ~2900 km below Earth's surface at the core-mantle boundary (6–10). The effects of the SAA in near-Earth space leads to an increase in the particles in radiation belts, which causes radiation damage to satellites and other spacecraft as well as being a hazard to astronauts (11). The fixity and existence of the SAA for times prior to the historical record remains controversial (12). Additionally, since the growth of the SAA is associated with an overall decay of the dipole field (7, 13–15), it has been interpreted by some as a precursor to a geomagnetic reversal (16–18).

The discussion about the longevity and locus of the SAA has inspired several studies, adding additional data and/or models, either focusing on historic timescales (12, 19–23), or on the South Atlantic region in the last 10 to 300 thousand years (kyr) (13, 24, 25). Data from Tristan da Cunha (Figure 1) from 90 to 46 thousand years ago (ka) show that the virtual axial dipole moment (VADM) measured at this island was weaker than elsewhere (24). Field models extending to 10 ka, show persistently higher secular variation activity in the Southern Hemisphere relative to the Northern Hemisphere (13). Similarly, it has been argued for enhanced secular variation in the region above the African Large Low Shear Velocity Province (LLSVP; Figure 1) located beneath a part of the South Atlantic region (25). Satellite and ground-based observations confirm high present-day secular variation in the Saint Helena area specifically (26). Several studies suggest a link between the irregular field behavior and heterogeneous heat flow across the Core Mantle Boundary (CMB) (10, 14, 22). Lowermost mantle viscosity is sufficiently high (> 10^{20} Pa.s (27)) to ensure that the margins of LLSVPs should be sufficiently stable on a timescale of at least 10 million years (Myr) (28) and potentially much longer (29), suggesting that the South Atlantic region should be showing persistently recurring anomalous behavior for at least that timescale.

Paleomagnetic data from Saint Helena

Existing paleomagnetic datasets (30) recovered from rocks less than ten million years old are scarce in the Southern Hemisphere, especially in the South Atlantic (Figure 1). Here we report a detailed study of paleosecular variation (PSV) from Saint Helena (Figure 2), which provides a uniquely ideal opportunity to test the hypothesis that geomagnetic variability is enhanced in the South Atlantic on a geological timescale. Saint Helena is an island in the South Atlantic consisting of two shield volcanoes that formed between ~8 and 11 million years ago (Ma) (31, 32). We performed paleodirectional analyses on 51 sites from 46 basalt flows from four different shields (SI Appendix 1 and Table S1), three from the younger volcano (SW volcano, upper/main/lower shield) and one from the older volcano (NE volcano, upper shield and breccias), and three thin dykes (late intrusions) (Figure 2).

Thermal and alternating field demagnetization experiments were performed on a minimum of five independently oriented specimens per rock unit (basalt flow or dyke). Characteristic components of remanent magnetization (ChRMs) were typically isolated by either step-wise thermal demagnetization between temperatures of 230 °C and 610 °C, or step-wise alternating field demagnetization between fields of 40 mT and 100 mT. ChRM directions show good agreement at the site level (e.g. 39 sites with minimum Fisher (33) precision parameter, $k > 50$, and 22 with $k > 100$ (Table S2)). Two positive baked contact tests using dykes at different locations and a positive reversal test (SI 2.4 & 2.9) support the primary nature of the ChRMs. To test the GAD hypothesis and perform PSV analysis, we applied the selection criteria at the site level of $k > 50$ and $n \geq 5$; 34 site mean directions passed the criteria and were included in the final dataset (Table S2; Figure 3a). These criteria were chosen to allow for comparison with the PSV10 dataset (30) (a dataset consisting of all the PSV data from the past 10 million years), for which $k > 50$ and $n \geq 4$ were used as selection criteria. More stringent selection criteria were also considered in SI 2.7 and will be discussed later on. All sites were corrected for plate motion since their emplacement, using the rotations of ref. (34), before calculating virtual geomagnetic poles (VGPs) (Figure 3b). Except for a few units locally rotated by later intrusive events, both field and palaeomagnetic evidence did not support any post-emplacement deformation affecting these rocks. The dataset comprises a record of at least six reversals, which is shown with a schematic magnetic stratigraphy overview in Figure S12, and the entirety passes a reversal test (SI 2.9, Figure S11). Two lava flows record directions that are categorized as transitional by a variable cut-off (Figure 3b)(35). The flows in the upper shield of the SE volcano (Prosperous Bay) capture a polarity reversal (Figure 3a, Supplemental Figure S12). Since we captured (at least) 6 reversals, or 7 chrons, we consider it likely that sufficient time was sampled overall to adequately represent secular variation.

Our mean pole (329.1° E, 81.1° N, A_{95} = 7.1°) is close to the geographic pole, once this is corrected for the tectonic motion of Saint Helena since 10 Ma. Therefore, the results are not more than marginally inconsistent with the GAD hypothesis being valid in this region (Figure 3b).

Evidence for enhanced secular variation

A remarkable feature of the Saint Helena dataset is that, despite directions being well-clustered at the within-site level (k > 50), indicating high-quality measurements, the VGP dispersion is high for its paleolatitude. To assess, quantitatively, the magnitude of directional variability evident in our dataset, we follow the approach and criteria of a recent global study of paleosecular variation over the last 10 Myr (30). Using our preferred dataset (N=34), we calculate a dispersion, S, of 21.9° ±3.5° (95% confidence range from 10,000 bootstraps (36)). Many of the flows were sampled in sequence, suggesting there is a risk of serial correlation (SC), which could underestimate secular variation. We investigated this by calculating new VGP dispersions for the dataset after accounting for possible serial correlation (SI 2.8). Following investigation of a range of selection criteria, cut-offs and correction of serial correlation, we conclude that the VGP dispersion may have varied between 18.4° and 22.6° (up to 30.4° when no cut-off is applied). In all cases, the value obtained is substantially higher than that expected value for this latitude (Figure S8, Table S3). When using a stricter selection criterion for the k value (100 instead of 50), together with the application of serial correlation, it reduces the size of our dataset to 16 after applying the Vandamme cut-off (34). The size of the dataset may be too low to yield a converged PSV estimate, although the time span of the dataset still ranges from ~8.8 - ~10.3 Ma. On the basis of the relative insensitivity of the anomalously high dispersion (18.4° – 22.6°) to the wide range of selection criteria approaches considered, we suggest that our main result is robust.

The present-day field (PDF) at Saint Helena, despite being one of the most deviant from GAD on the planet (angular distance 26.3°, Figure 1), would not be considered an outlier relative to other instantaneous field records for the past 10 Myr (Figure 3b). Indeed, there are four non-transitional sites from Saint Helena, that are further than the PDF magnetic pole from the geographic pole. That the location of the PDF pole does not place it outside of the “normal” range of secular variation for this region suggests that the SAA does not represent an anomaly of sufficient magnitude to herald an upcoming reversal (e.g. ref. 18).

In Figure 4a, the dispersion of our dataset is compared to PSV10 (30) grouped into 10° latitude bins for the Atlantic hemisphere (-90°E to 90°E) and Pacific hemispheres separately (Figure 1). One way to describe VGP dispersion is the use of Model G (37), which predicts VGP dispersion for a given

paleolatitude (λ) with the following equation: $S^2 = a^2 + (b\lambda)^2$ (a = VGP dispersion at the equator, b = paleolatitude dependent increase in dispersion). The Model G style fit (Figure 4) of ref. (38) of the PSV10 dataset (30), determined values of a = 11.3 +1.3/-1.1 and b = 0.27 +0.04/0.08 (38) and is hereafter referred to as the Model G fit. Since no data are published from the Atlantic hemisphere between 10° S and 20° S that meet the PSV10 criteria, the Saint Helena dataset forms an entire new latitude bin. This data point (VGP dispersion of 21.9° for k > 50, n ≥ 5, N = 34, at a paleolatitude of 19.8° S) forms a distinctive outlier from the Model G fit to PSV10 (38) and the overall dataset from PSV10 (30). The difference of at least 9° between Saint Helena and the Model G fit, shows that geomagnetic secular variation was anomalously high around Saint Helena between ~8 and 11 Ma. The only other bin associated, with uncertainties that do not overlap with those of the Model G fit is below the trend. This likely indicates that the time period in which these rocks formed was either one of unusual high field stability or was too short a time interval to fully capture secular variation. The finding that VGP dispersion is at the extreme high end of the range of measurements for this latitude in the Atlantic persists even if no cut-off is applied to the PSV10 dataset (Figure S9).

When the PSV10 data set are considered by locality rather than in latitudinal bins (SI 3), several more outliers are evident (Figure 4b). Most of these are at mid- to high latitudes both northern and southern, or are from single-polarity studies with much lower dispersion values than expected (potentially caused by temporal under-sampling and therefore not capturing secular variation (39)). The single other high outlier from low latitudes (< ±30°) comes from the island of Martinique (40) in the North Atlantic (#1 in Figures 1 and 4b, S = 25.9° +7.1° / -8.2°). The authors of that study (40) suggest that the high dispersion is due to the small number of sites (N = 14), which has been shown to produce erratic values (39). In Figure 4a, no outlier is found for this latitude band because the island of Martinique has been combined with 3 others, one from Cape Verde (41) (#2 in Figures 1 and 4) with S = 13.7° + 2.5° / -2.6° and N = 27, one from Costa Rica (42) (#3 in Figures 1 and 4) with S = 14.8° +2.7° / -2.8° and N = 29 (only half of the sites from the Costa Rica study are in the latitude bin with Martinique, the others just fall in the 0° - 10° N bin), and one from Guadeloupe Island (43) (#4 in Figures 1 and 4) with S = 9.4° +2.1° / -2.3° and N = 22. Guadeloupe Island is only 130 km away from Martinique Island and they are both from rocks that are no older than 2 Ma, thus the difference in VGP dispersion would support the assertion of the authors of ref. (40): the high scatter value may not be representative of the time-averaged field. We therefore find no strong grounds for suggesting that the anomalous behavior detected at Saint Helena extends far northwards from the South Atlantic. This is supported by low VGP dispersion values from São Tomé (#5 in Figures 1 and 4, 11.1° + 1.9°/ -2.0°; N = 38) (44) and Fernando de Noronha (#6 in Figures, 11.5° +1.9°/ -2.0°; N = 37)

(45), also at low latitudes in the Atlantic, which are consistent with the Model G fit and PSV10 (Figure 4b). Since both of these localities have captured long time intervals (5 – 9 Ma and 1.8 – 12 Ma for São Tomé and Fernando de Noronha, respectively (44, 45)), they suggest a long-lived northern limit to the anomalous behavior of the South Atlantic region around the Equator. This is supported by the other low latitude Atlantic results that fall on or below the trend of the Model G fit (Figure 4b).

Two studies have been performed at a similar latitude to our study on Réunion (46, 47), (#7 in Figures 1 and 4, mean paleolatitude of -21.2°) yielding S = 12.5° +1.5° / -1.4°; N = 61 (combination of both studies). Réunion is an island in the Atlantic hemisphere, where, according to the *gufm1* (48) model, the flux patch responsible for the present-day South Atlantic Anomaly was located prior to moving westwards. The question of whether the anomalous behavior detected at Saint Helena could also have been present further to the east remains an open one, however, because all the Réunion flows have ages within the last 50 kyr, this time interval may be too short and/or under-sampled to comment on the existence of irregular behavior in the field eastwards of the South Atlantic.

Localities in the PSV10 dataset that are further south than Saint Helena and Réunion in the Atlantic Hemisphere are in Chile, Argentina and Western Antarctica (Figure 1), and thus too far west from the current South Atlantic Anomaly features to constrain its southern limit. A paleointensity dataset from Tristan da Cunha (37° S; 12° W; Figure 1), gives anomalously low intensity values (24), suggesting that there is not a strict southern limit known yet. VGP dispersion from Tristan da Cunha was not reported in PSV10, but we used their published data to calculate a VGP dispersion of 19.8° (+3.7/-4.0) with N = 23 (corrected for serial correlation as suggested by ref. (24). This VGP dispersion value does fall above the trend from the Model G fit (Figure 4b) further supporting that anomalous behavior may extend this far south.

Implications for the deep Earth

Our results support recent studies (10, 13, 14, 20, 22, 24, 25), arguing for the long-lived recurrence of anomalous behavior in the South Atlantic region but extend the associated timeframe from thousands to millions of years, thus supporting a plausible connection to lowermost mantle conditions. Tarduno et al. (22) suggested that recurrent intensity drops and rapid directional changes in southern Africa, between 1600 AD and 1000 AD, were related to the margin of the African LLSVP (Figure 1) at the CMB. This LLSVP's edge coincides with a reverse flux patch in the present Earth's magnetic field on the CMB. They propose that the steep edge of the LLSVP stimulates the formation of small structures or vortices in the outer core flow. This small scale turbulence promotes the

leaking of reversed polarity magnetic flux bundles upwards, producing pairs of reversed and normal patches on the CMB (22). Lowermost mantle viscosity is sufficiently high to ensure that the margins of LLSVPs should be stable on a timescale of at least 10 million years and potentially much longer (27, 29). Therefore, this mechanism predicts and requires anomalous secular variation in the southern Atlantic-African region on the timescales that our new data support. The concept of the lowermost mantle exerting control on the geodynamo and magnetic field on a timescale of millions of year is supported at least during intervals of reduced dipole moment (49).

An alternate hypothesis relates to the claim that Earth's outer core may presently contain a planetary-scale eccentric gyre (14, 50–54) that produces strong westward drift of flux patches at low latitudes on the CMB. The eccentricity of the gyre would cause focused magnetic variations in the longitudinal section beneath the Atlantic, where the gyre reaches the core surface (14). Aubert et al. (14) dynamically modelled the eccentricity of the gyre as a consequence of asymmetric buoyancy release from the inner core boundary in a region whose location (beneath Indonesia) was dictated by the patch of seismically-inferred global-maximum heat flux across the CMB. This model predicts that it is not just the South Atlantic, but the entire low latitude portion of the Atlantic hemisphere that displays enhanced geomagnetic variability, a contention which they argue is supported with secular variation data from *gufm1* (14, 48) showing higher secular variation energy in the Atlantic hemisphere compared to the Pacific hemisphere. Since the heat flux anomaly is presumed to be a product of sustained subduction, this phenomenon would again be long-lived and expected to be visible in paleomagnetic datasets spanning ten million years or longer. Although the separate localities from the Atlantic hemisphere do not all support this model (potentially due to the short time interval that they sampled, like Réunion), it is noticeable that, from all the Pacific data, only 27% (3/11) of the latitude bins plot above or on the Model G fit (37, 38), whereas 64% (9/14) of the Atlantic latitude bins plot above or on it (Figure 4a). This observation is marginally consistent with enhanced secular variation in the Atlantic hemisphere and does not rule out the persistence of an eccentric gyre, similar to today, on geological timescales.

The VGP dispersion recorded by Saint Helena lavas (21.9°), is significantly higher (>9°) than the predicted dispersion from the Model G fit (38), based on the PSV10 dataset (30) (Figure 4). This indicates that the magnetic field was showing more irregular behavior in the South Atlantic than in other regions since 10 Ma. Our results strongly support and enhance recent claims over the persistent recurrence of geomagnetic anomalies in this region (22, 24) and may add weight to the argument that the low latitude Atlantic hemisphere experiences stronger secular variation than its Pacific counterpart on geological timescales (13, 14, 25). Explanations for long-lived geomagnetic

anomalies rely to some extent on the influence of the heterogeneous lowermost mantle on the underlying core flow. This study therefore constitutes further evidence of core-mantle interaction affecting the geodynamo process. While we did obtain a mean VGP marginally offset from the geographic pole, we otherwise found no convincing evidence to indicate that the enhanced secular variation at Saint Helena fed into any substantial anomaly in the time-averaged field. We consider that this should be reassuring to the geologic and paleogeographic community who rely on the GAD assumption to perform continental reconstructions. Finally, that the present day field pole produced at Saint Helena sits inside the range of nominally non-transitional VGPs produced over a protracted period in the past does not support the somewhat controversial hypothesis that the present-day SAA is a recent feature, linked to the overall decay of the field and a signal of an incipient polarity reversal.

Methods

At each of the 52 sites, generally a single flow or dyke (except for flow LH20a-20c which are all the same flow, SB01 and SB02 which are from the same flow, and SB03 which samples 2 separate dykes), 5 to 10 drill cores samples of 2.5 cm in diameter along with, commonly, at least one oriented or non-oriented hand sample, were collected. When possible, we collected samples from the lower, middle and upper part of each flow. All drilled paleomagnetic core samples were oriented with a sun and/or magnetic compass (Table S2). When sun compass orientations were not possible due to cloud cover, we assume the magnetic orientation as correct, based on the minimal differences between magnetic and sun-compass orientation for the other samples (further sampling and geology of Saint Helena can be found in SI 1). Paleomagnetic experiments were performed at the Geomagnetism Lab, University of Liverpool. A combination of MMTD24 thermal demagnetizer, 2G Cryogenic magnetometer with RAPID sample handling system and a JR6 spinner magnetometer were used. A total of 248 specimens from 225 cores were stepwise demagnetized. 99 specimens were thermally demagnetized (10 – 17 steps up to 620 °C or complete demagnetization), and 149 specimens were demagnetized by an alternating field (AF, 12 steps, up to 100 mT). For the analyses, we used the platform-independent portal paleomagnetism.org (55). The results are shown in orthogonal projection plots or “Zijderveld” plots (SI 2.3; Figure S3) (56) and equal area projections. Principal component analysis (PCA) was used to interpret the characteristic remanent magnetization (ChRM) (57). Generally, a free-floating PCA was used. Samples with a maximum angular distance (MAD) over 14° were not used for the interpretation. For within site dispersion a minimum k value of 5 and n value of 5 were needed for the results to be included in the VGP dataset. Due to the methods chosen for demagnetization and analyses, all our results can be given Demagnetization Code 5 (DC5) (58). Per site or cooling unit Fisher mean directions (33) were calculated with an α_{95} confidence interval (59). We calculated the VGP latitude and longitude for each site after using the NNR-MORVEL56 model (34) to correct for plate motion. We calculated the mean VGP and the dispersion (S) using Vandamme cut-off (35) or 45° cut-off. The formula used for the dispersion is:

$$S_b = \sqrt{\frac{1}{N-1}\sum_{i=1}^{N}\left(\Delta_i^2 - \frac{S_{w_i}^2}{N_{S_i}}\right)}$$

Here, Δ_i represents the angular deviation of *i*th site's VGP to the mean of the VGPs, N is the number of sites, S_w is the within site dispersion calculated from k and N_S is the number of samples within the site. S_b represents the dispersion of the magnetic signal, after correcting for the within-site dispersion S_w determined from N_s samples (60, 61).

Data availability The full data set including measurements, site mean directions and VGPs, will be made public in the MagIC database. To access these data, go to https://earthref.org/MagIC/16824/5636af20-667f-48c4-886e-a3f73eaf8778

Acknowledgements This work was supported by The Leverhulme Trust (RL-2016-80). We would like to thank the Saint Helena Council and David Pryce for their assistance with field work, and Courtney Sprain and Joe Heraty for assistance with thermal and AF demagnetization experiments. We also thank Ian Baker for very helpful discussions on the geology of Saint Helena. We would like to thank the two anonymous reviewers for their helpful comments and suggestions.

References

1. C. L. Johnson, C. G. Constable, The time-averaged geomagnetic field: Global and regional biases for 0-5 Ma. *Geophys. J. Int.* **131**, 643–666 (1997).

2. D. A. D. Evans, Proterozoic low orbital obliquity and axial-dipolar geomagnetic field from evaporite palaeolatitudes. *Nature* **444**, 51–55 (2006).

3. M. Korte, C. Constable, F. Donadini, R. Holme, Reconstructing the Holocene geomagnetic field. *Earth Planet. Sci. Lett.* **312**, 497–505 (2011).

4. A. Nilsson, R. Holme, M. Korte, N. Suttie, M. Hill, Reconstructing holocene geomagnetic field variation: New methods, models and implications. *Geophys. J. Int.* **198**, 229–248 (2014).

5. E. Thébault, *et al.*, International geomagnetic reference field: The 12th generation international geomagnetic reference field - The twelfth generation. *Earth, Planets Sp.* **67** (2015).

6. D. Gubbins, Mechanism for geomagnetic polarity reversals. *Nature* **326**, 167–169 (1987).

7. D. Gubbins, A. L. Jones, C. C. Finlay, Fall in Earth's Magnetic Field Is Erratic. *Science (80-.).* **312**, 900 LP – 902 (2006).

8. G. Hulot, C. Eymin, B. Langlais, M. Mandea, N. Olsen, Small-scale structure of the geodynamo inferred from Oersted and Magsat satellite data. *Nature* **416**, 620–623 (2002).

9. G. A. Hartmann, I. G. Pacca, Time evolution of the South Atlantic Magnetic Anomaly. *An. Acad. Bras. Cienc.* **81**, 243–255 (2009).

10. F. Terra-Nova, H. Amit, G. Choblet, Preferred locations of weak surface field in numerical dynamos with heterogeneous core-mantle boundary heat flux: Consequences for the South Atlantic Anomaly. *Geophys. J. Int.* **217**, 1179–1199 (2019).

11. J. R. Heirtzler, The future of the South Atlantic anomaly and implications for radiation damage in space. *J. Atmos. Solar-Terrestrial Phys.* **64**, 1701–1708 (2002).

12. S. A. Campuzano, M. Gómez-Paccard, F. J. Pavón-Carrasco, M. L. Osete, Emergence and evolution of the South Atlantic Anomaly revealed by the new paleomagnetic reconstruction SHAWQ2k. *Earth*

Planet. Sci. Lett. **512**, 17–26 (2019).

13. C. Constable, M. Korte, S. Panovska, Persistent high paleosecular variation activity in southern hemisphere for at least 10 000 years. *Earth Planet. Sci. Lett.* **453**, 78–86 (2016).

14. J. Aubert, C. C. Finlay, A. Fournier, Bottom-up control of geomagnetic secular variation by the Earth's inner core. *Nature* **502**, 219–223 (2013).

15. C. C. Finlay, J. Aubert, N. Gillet, Gyre-driven decay of the Earth's magnetic dipole. *Nat. Commun.* **7** (2016).

16. A. De Santis, E. Qamili, L. Wu, Toward a possible next geomagnetic transition? *Nat. Hazards Earth Syst. Sci.* **13**, 3395–3403 (2013).

17. F. J. Pavón-Carrasco, A. De Santis, The South Atlantic anomaly: The key for a possible geomagnetic reversal. *Front. Earth Sci.* **4** (2016).

18. C. Laj, C. Kissel, An impending geomagnetic transition? Hints from the past. *Front. Earth Sci.* **3** (2015).

19. W. Poletti, A. J. Biggin, R. I. F. Trindade, G. A. Hartmann, F. Terra-Nova, Continuous millennial decrease of the Earth's magnetic axial dipole. *Phys. Earth Planet. Inter.* **274**, 72–86 (2018).

20. V. J. Hare, *et al.*, New Archeomagnetic Directional Records From Iron Age Southern Africa (ca. 425–1550 CE) and Implications for the South Atlantic Anomaly. *Geophys. Res. Lett.* **45**, 1361–1369 (2018).

21. G. A. Hartmann, W. Poletti, R. I. F. Trindade, L. M. Ferreira, P. L. M. Sanches, New archeointensity data from South Brazil and the influence of the South Atlantic Anomaly in South America. *Earth Planet. Sci. Lett.* **512**, 124–133 (2019).

22. J. A. Tarduno, *et al.*, Antiquity of the South Atlantic Anomaly and evidence for top-down control on the geodynamo. *Nat. Commun.* **6** (2015).

23. M. Brown, M. Korte, R. Holme, I. Wardinski, S. Gunnarson, Earth's magnetic field is probably not reversing. *Proc. Natl. Acad. Sci. U. S. A.* **115**, 5111–5116 (2018).

24. J. Shah, *et al.*, Palaeomagnetic evidence for the persistence or recurrence of geomagnetic main field anomalies in the South Atlantic. *Earth Planet. Sci. Lett.* **441**, 113–124 (2016).

25. L. B. Ziegler, C. G. Constable, Testing the geocentric axial dipole hypothesis using regional paleomagnetic intensity records from 0 to 300 ka. *Earth Planet. Sci. Lett.* **423**, 48–56 (2015).

26. R. Holme, N. Olsen, F. L. Bairstow, Mapping geomagnetic secular variation at the core-mantle boundary. *Geophys. J. Int.* **186**, 521–528 (2011).

27. D. G. van der Meer, D. J. J. van Hinsbergen, W. Spakman, Atlas of the underworld: Slab remnants in the mantle, their sinking history, and a new outlook on lower mantle viscosity. *Tectonophysics* **723**, 309–448 (2018).

28. R. K. Bono, J. A. Tarduno, H.-P. Bunge, Hotspot motion caused the Hawaiian-Emperor Bend and LLSVPs are not fixed. *Nat. Commun.* **10** (2019).

29. T. H. Torsvik, K. Burke, B. Steinberger, S. J. Webb, L. D. Ashwal, Diamonds sampled by plumes from the core-mantle boundary. *Nature* **466**, 352–355 (2010).

30. G. Cromwell, C. L. Johnson, L. Tauxe, C. G. Constable, N. A. Jarboe, PSV10: A Global Data Set for 0–10 Ma Time-Averaged Field and Paleosecular Variation Studies. *Geochemistry, Geophys. Geosystems* **19**, 1533–1558 (2018).

31. T. Hanyu, *et al.*, Isotope evolution in the HIMU reservoir beneath St. Helena: Implications for the mantle recycling of U and Th. *Geochim. Cosmochim. Acta* **143**, 232–252 (2014).

32. I. Baker, N. H. Gale, J. Simons, Geochronology of the St Helena volcanoes. *Nature* **215**, 1451–1456 (1967).

33. R. Fisher, Dispersion on a Sphere. *Proc. R. Soc. A Math. Phys. Eng. Sci.* **217**, 295–305 (1953).

34. D. F. Argus, R. G. Gordon, C. Demets, Geologically current motion of 56 plates relative to the no-net-rotation reference frame. *Geochemistry, Geophys. Geosystems* **12** (2011).

35. D. Vandamme, A new method to determine paleosecular variation. *Phys. Earth Planet. Inter.* **85**, 131–142 (1994).

36. B. Efron, R. J. Tibshirani, *An Introduction to the Bootstrap* (CRC Press, 1994) (January 17, 2020).

37. M. W. McElhinny, P. L. McFadden, Palaeosecular variation over the past 5 Myr based on a new generalized database. *Geophys. J. Int.* **131**, 240–252 (1997).

38. P. V. Doubrovine, *et al.*, Latitude Dependence of Geomagnetic Paleosecular Variation and its Relation to the Frequency of Magnetic Reversals: Observations From the Cretaceous and Jurassic. *Geochemistry, Geophys. Geosystems* **20**, 1240–1279 (2019).

39. A. J. Biggin, D. J. J. van Hinsbergen, C. G. Langereis, G. B. Straathof, M. H. L. Deenen, Geomagnetic secular variation in the Cretaceous Normal Superchron and in the Jurassic. *Phys. Earth Planet. Inter.* **169**, 3–19 (2008).

40. C. Tanty, J. Carlut, J.-P. Valet, A. Germa, Palaeosecular variation recorded by 9 ka to 2.5-Ma-old lavas from Martinique Island: new evidence for the La Palma aborted reversal 617 ka ago. *Geophys. J. Int.* **200**, 915–932 (2015).

41. M. C. Brown, *et al.*, No evidence for Brunhes age excursions, Santo Antão, Cape Verde. *Earth Planet. Sci. Lett.* **287**, 100–115 (2009).

42. G. Cromwell, C. G. Constable, H. Staudigel, L. Tauxe, P. Gans, Revised and updated paleomagnetic results from Costa Rica. *Geochemistry, Geophys. Geosystems* **14**, 3379–3388 (2013).

43. J. Carlut, X. Quidelleur, V. Courtillot, G. Boudon, Paleomagnetic directions and K/Ar dating of 0 to 1 Ma lava flows from La Guadeloupe Island (French West Indies): Implications for time-averaged field models. *J. Geophys. Res. Solid Earth* **105**, 835–849 (2000).

44. N. D. Opdyke, D. V. Kent, D. A. Foster, K. Huang, Paleomagnetism of Miocene volcanics on Sao Tome: Paleosecular variation at the Equator and a comparison to its latitudinal dependence over the last 5 Myr. *Geochemistry, Geophys. Geosystems* **16**, 3870–3882 (2015).

45. R. Leonhardt, J. Matzka, E. A. Menor, Absolute paleointensities and paleodirections of miocene and pliocene lavas from Fernando de Noronha, Brazil. *Phys. Earth Planet. Inter.* **139**, 285–303 (2003).

46. A. Raïs, C. Laj, J. Surmont, P. Y. Gillot, H. Guillou, Geomagnetic field intensity between 70 000 and 130 000 years B.P. from a volcanic sequence on La Réunion, Indian Ocean. *Earth Planet. Sci. Lett.* **140**, 173–189 (1996).

47. A. Chauvin, P. Y. Gillot, N. Bonhommet, Paleointensity of the Earth's magnetic field recorded by two late Quaternary volcanic sequences at the island of La Reunion (Indian Ocean). *J. Geophys. Res.* **96**, 1981–2006 (1991).

48. A. Jackson, A. R. T. Jonkers, M. R. Walker, Four centuries of geomagnetic secular variation from historical records. *Philos. Trans. R. Soc. A Math. Phys. Eng. Sci.* **358**, 957–990 (2000).

49. K. A. Hoffman, P. Camps, M. Carlton, Rare Paleomagnetic Evidence of Long-term Mantle Control of the Geodynamo and Possible Role of the NAD-field in the Reversal Process. *Geophys. J. Int.*, ggz480.

50. N. Gillet, D. Jault, C. C. Finlay, Planetary gyre, time-dependent eddies, torsional waves, and equatorial jets at the Earth's core surface. *J. Geophys. Res. Solid Earth* **120**, 3991–4013 (2015).

51. N. Gillet, M. A. Pais, D. Jault, Ensemble inversion of time-dependent core flow models. *Geochemistry, Geophys. Geosystems* **10** (2009).

52. J. Baerenzung, M. Holschneider, V. Lesur, Bayesian inversion for the filtered flow at the Earth's core-mantle boundary. *J. Geophys. Res. Solid Earth* **119**, 2695–2720 (2014).

53. M. A. Pais, D. Jault, Quasi-geostrophic flows responsible for the secular variation of the Earth's magnetic field. *Geophys. J. Int.* **173**, 421–443 (2008).

54. J. Aubert, Recent geomagnetic variations and the force balance in Earth's core. *Geophys. J. Int.* (2020) https:/doi.org/10.1093/gji/ggaa007.

55. M. R. Koymans, C. G. Langereis, D. Pastor-Galán, D. J. J. van Hinsbergen, Paleomagnetism.org: An online multi-platform open source environment for paleomagnetic data analysis. *Comput. Geosci.* **93**, 127–137 (2016).

56. J. D. A. Zijderveld, *A. C. Demagnetization of Rocks: Analysis of Results*, K. M. C. and S. K. R. D. W. Collinson, Ed. (Elsevier, Amsterdam, 1967).

57. J. L. Kirschvink, The least-squares line and plane and the analysis of palaeomagnetic data. *Geophys. J. R. Astron. Soc.* **62**, 699–718 (1980).

58. M. W. McElhinny, P. L. McFadden, *Paleomagnetism: Continents and oceans* (San Diego: Academic Press., 2000).

59. M. H. L. Deenen, C. G. Langereis, D. J. J. van Hinsbergen, A. J. Biggin, Geomagnetic secular variation and the statistics of palaeomagnetic directions. *Geophys. J. Int.* **186**, 509–520 (2011).

60. C. L. Johnson, *et al.*, Recent investigations of the 0-5 Ma geomagnetic field recorded by lava flows. *Geochemistry, Geophys. Geosystems* **9** (2008).

61. A. R. Dominguez, R. Van der Voo, Secular variation of the middle and late Miocene geomagnetic field recorded by the Columbia River Basalt Group in Oregon, Idaho and Washington, USA. *Geophys. J. Int.* **197**, 1299–1320 (2014).

62. G. E. Shephard, K. J. Matthews, K. Hosseini, M. Domeier, On the consistency of seismically imaged lower mantle slabs. *Sci. Rep.* **7**, 1–17 (2017).

Figure 1; Present day magnetic field. Angular distance in degrees from GAD per virtual geomagnetic pole from IGRF12 for 2015 (4). The purple dashed lines indicate the boundary between the Atlantic Hemisphere (AH) and the Pacific Hemisphere (PH). The black line marks a suggested boundary of the African and Pacific Large Low Shear Velocity Province (LLSVP) at the Core Mantle Boundary (CMB), defined as a region with below average shear wave velocity at 2850 km depth in at least 10 of 18 mantle tomography models, as interpreted by voting map model (62). Green square marks the paleolocation of Tristan da Cunha (discussed in text). Red dots mark PSV10 locality paleolocations (SI 3, Table S4) (30). The numbered locations mark specific localities discussed in the text (1 = Martinique, 2 = Cape Verde, 3 = Costa Rica, 4 = Guadeloupe, 5 = São Tomé, 6 = Fernando de Noronha and 7 = Réunion). The magenta star is marking the present location of Saint Helena, and the blue star marks the paleolocation of Saint Helena. All paleolocations are calculated using the NNR-morvel56 model (34) (Methods section and SI 2.6).

Figure 2; Geologic map of Saint Helena (North is up) with sampling locations for this study; Bank's Valley (BV) is from the north eastern volcano (NE). Ladder Hill (LH), Cambrian House (CH) (combined with LH in Figure 3), Prosperous Bay (PB), Airport Road (AP) (combined with PB in Figure 3), Porch's Gate (PG) and Sandy Bay (SB) are from the younger, south western volcano (SW). Adapted from ref. (32).

Figure 3; Summary of paleomagnetic data from Saint Helena. a) The Fisher (33) mean directions per site with a $k \geq 50$ and $n \geq 5$. Transitional (based on the Vandamme cut-off (35) sites (dashed ellipses) are shown but not used for PSV analysis. b) Site mean virtual geomagnetic poles in red, with the sites excluded by the Vandamme cut-off (44.4°, shown with green dash line) in orange. The VGP for the present-day field (PDF) is shown in blue. The Fisher (33) mean for all sites with 95% confidence interval are shown with a purple star and purple circle.

Figure 4; Comparison of Saint Helena data with PSV10. a) The VGP dispersions of the PSV10 dataset (30) plotted against latitude. VGP dispersions are calculated for Pacific and Atlantic hemispheres (seperation at -90° E and 90° E), 10° latitude bins. A Vandamme cut-off (35) was used and $k > 50$ and $n \geq 4$ as selection criteria per site (except for Saint Helena, for which $k > 50$ and $n \geq 5$ was used). The numbers indicate the amount of sites in that latitude bin. b) VGP dispersion of the PSV10 dataset (30) per locality (SI 3, Table S4). VGP dispersion for Tristan da Cunha was added as the green square. The same selection criteria and cut-off as in a. Localities that are mentioned specifically in the text are numbered same as in Figure 1 (1 = Martinique, 2 = Cape Verde, 3 = Costa Rica, 4 = Guadeloupe, 5 = São Tomé, 6 = Fernando de Noronha and 7 = Réunion). In both figures the red star is Saint Helena, and the pink dashed line is the Model G fit (fitted to PSV10 (see text) with 95% uncertainties, shaded area around the model G curve) (37, 38).

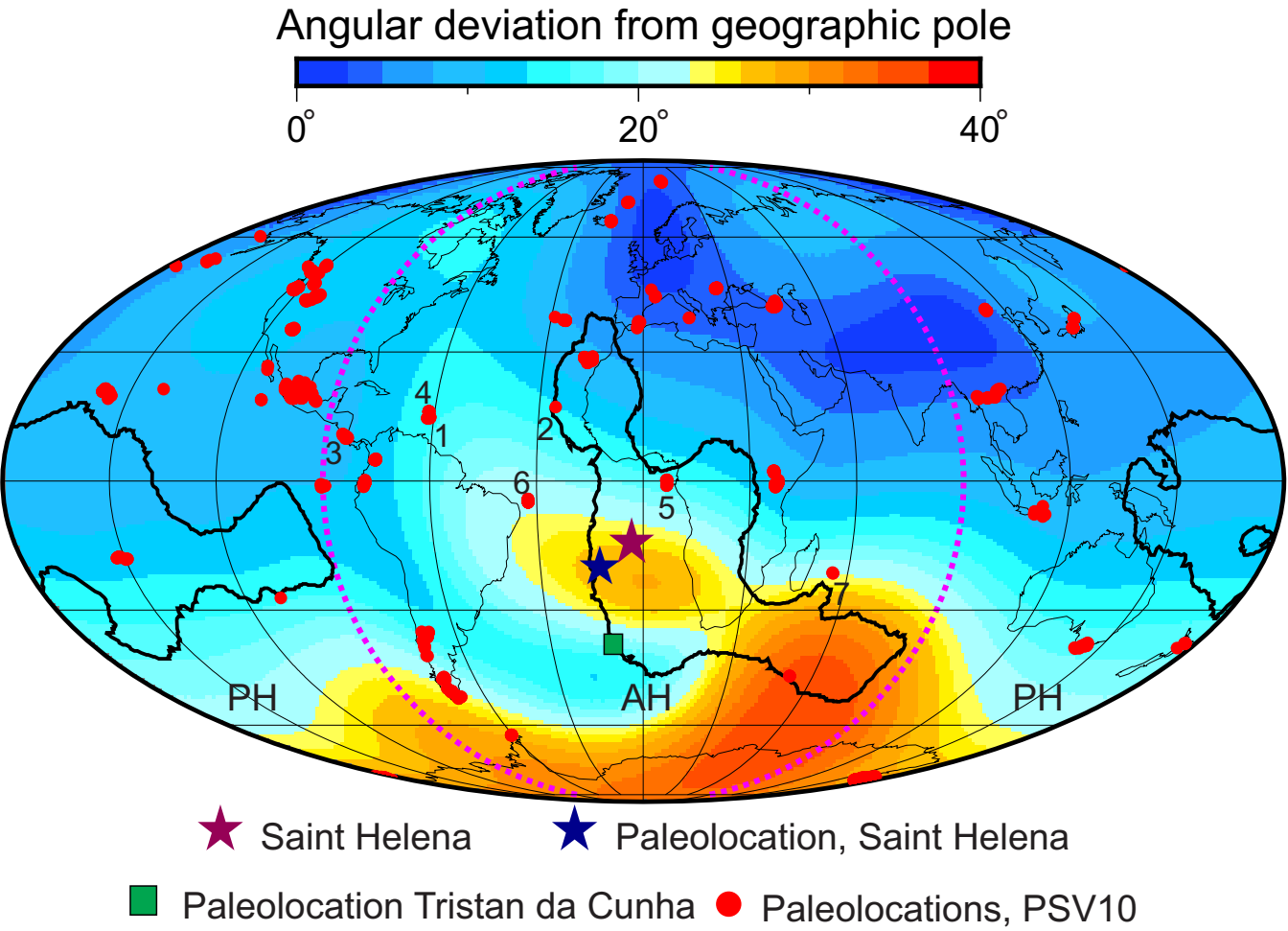
Angular deviation from geographic pole
0°
20°
40°
4
1
2
3
6
5
7
PH
AH
PH
Saint Helena
Paleolocation, Saint Helena
Paleolocation Tristan da Cunha
Paleolocations, PSV10

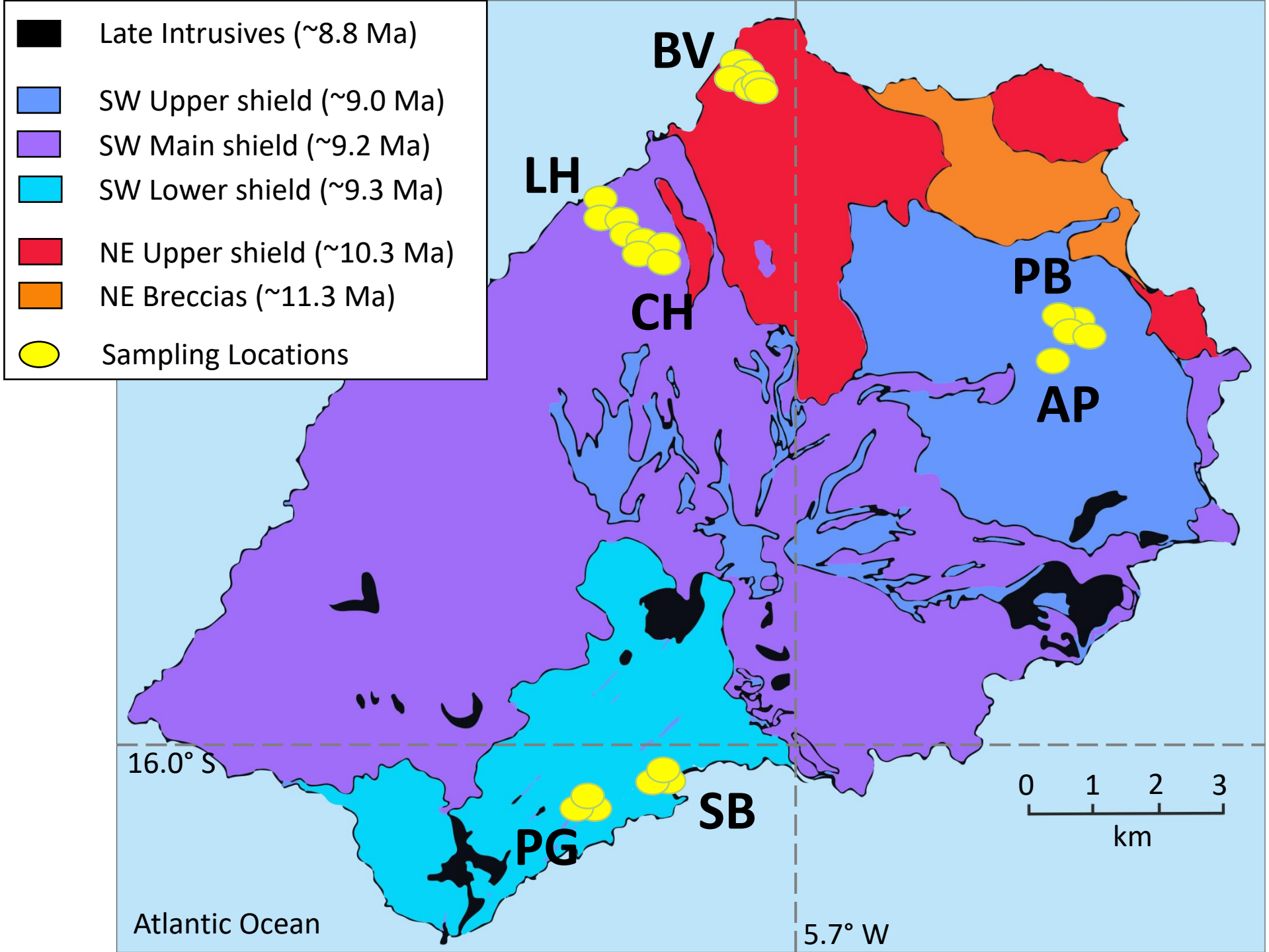
Late Intrusives (~8.8 Ma)
SW Upper shield (~9.0 Ma)
SW Main shield (~9.2 Ma)
SW Lower shield (~9.3 Ma)
NE Upper shield (~10.3 Ma)
NE Breccias (~11.3 Ma)
Sampling Locations
BV
LH
CH
PB
AP
SB
PG
16.0° S
5.7° W
Atlantic Ocean
0 1 2 3
km

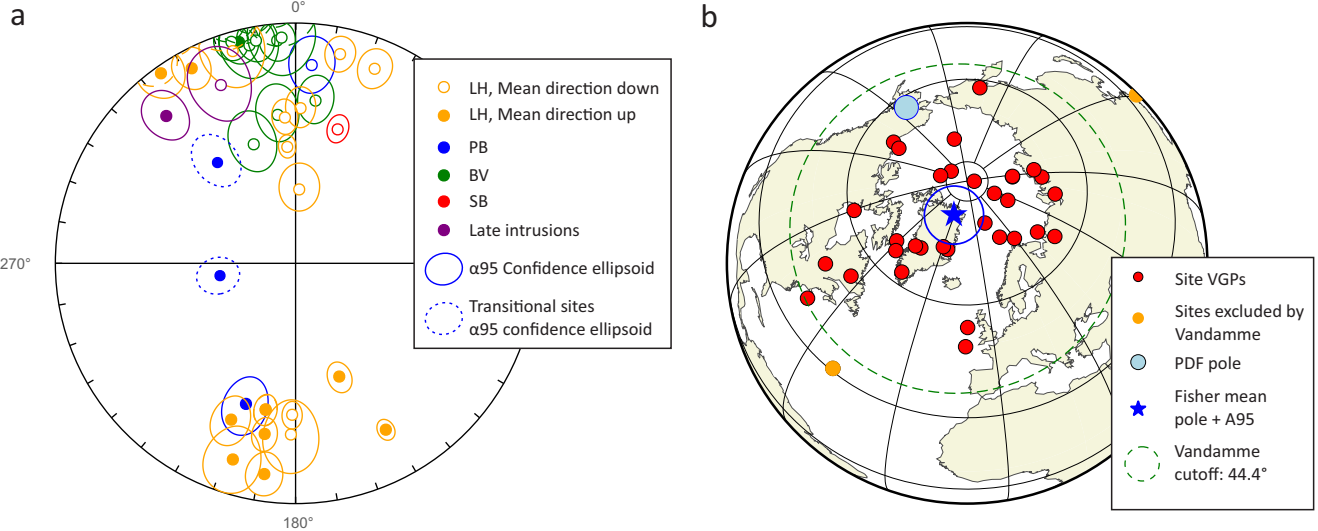
a
0°
270°
180°
LH, Mean direction down
LH, Mean direction up
PB
BV
SB
Late intrusions
α95 Confidence ellipsoid
Transitional sites
α95 confidence ellipsoid
b
Site VGPs
Sites excluded by Vandamme
PDF pole
Fisher mean pole + A95
Vandamme cutoff: 44.4°

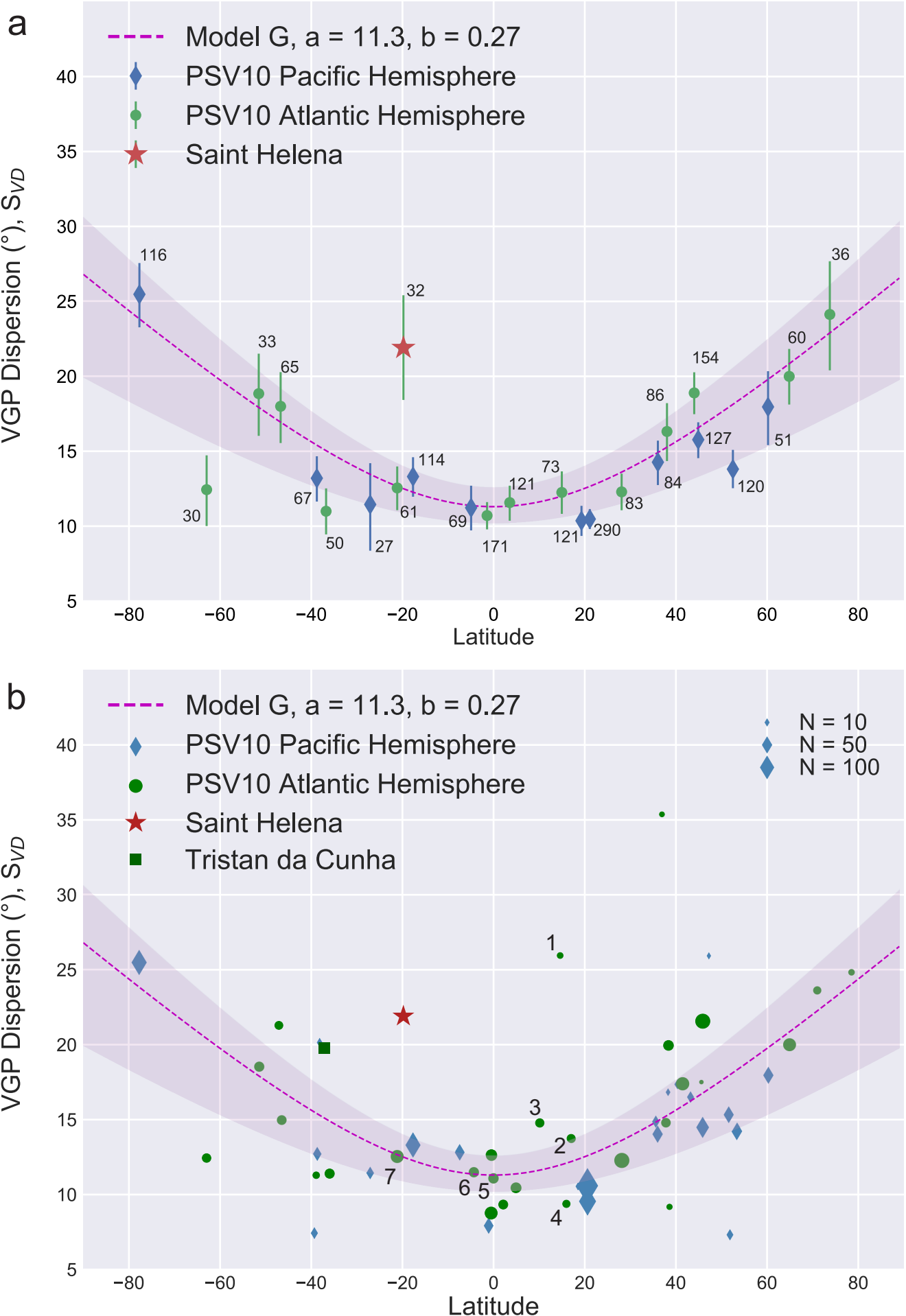
a
Model G, a = 11.3, b = 0.27
PSV10 Pacific Hemisphere
PSV10 Atlantic Hemisphere
Saint Helena
VGP Dispersion (°), S_{VD}
Latitude
116
32
33
65
36
60
154
86
127
51
114
73
121
84
120
30
67
61
83
69
121
290
50
27
171
b
Model G, a = 11.3, b = 0.27
PSV10 Pacific Hemisphere
PSV10 Atlantic Hemisphere
Saint Helena
Tristan da Cunha
N = 10
N = 50
N = 100
VGP Dispersion (°), S_{VD}
Latitude
1
2
3
4
5
6
7